Journal of Sound and Vibration (1998) **218**(3), 361–387
Article No. sv981862

VIBRATIONS OF CYLINDRICAL PIPES AND OPEN SHELLS

N. M. Price, M. Liu and R. Eatock Taylor

Department of Engineering Science, *University of Oxford*, *Parks Road*, *Oxford OX*1 3*PJ*, *England*

AND

A. J. Keane

Department of Mechanical Engineering, *University of Southampton*, *Highfield*, *Southampton SO*17 1*BJ*, *England*

(*Received* 30 *October* 1996, *and in final form* 25 *March* 1998)

The theory of vibrations in cylindrical pipes within the context of thin shell theory is reviewed. Beginning with a summary of the thin shell equations of motion and their application to cylindrical shells, solutions are obtained for a specific example of a typical pipe for each of several thin shell theories including: Donnell's theory, Love's theory and an improved theory which includes the effects of rotary inertia and transverse shear. For comparison, finite element (FE) models of the pipe are also constructed. To investigate the effect of shell curvature on the thin shell equations, various models of open shells evolving from a curved plate are also examined. The FE results are shown to agree well with those from the improved theory over the range of frequencies studied (the lowest 15–20 modes), though the time for their computation when using commercial FE software is three orders of magnitude longer.

1. INTRODUCTION

Pipe-work is common on many offshore structures, with recent years seeing the advent of larger, thinner walled pipes made of new materials. Such pipes may suffer fatigue failure by processes not previously encountered in smaller diameter, thicker walled systems and this makes a review of pipe theory, i.e., thin shell theory, worthwhile. Industry currently uses Finite Element (FE) analysis to model such systems which, while general purpose, does have certain shortcomings. The FE method depends heavily upon numerical procedures which demand large, fast computational facilities in order to deal with mathematical models representing very detailed idealizations of the physical structures. The computational demands increase with structural and material complexity and with analysis frequency range. Even today, with computational methods highly developed and optimized and escalating computing power, it is generally not practicable to predict the detailed vibrational behaviour of such structures beyond the first twenty or so

0022–460X/98/480361 + 27 $30.00/0

vibrational modes. In addition, as the complexity of such numerical methods increases the would-be user needs to be wary of the many pitfalls associated with the use of large packages of software. Analytic solutions of simpler problems may then provide a check against which to measure the accuracy of more complex numerical methods.

The work presented here forms part of a larger project examining vibration energy flow within systems of pipe-work, the study of which is generally not amenable to analysis by using FE methods. Instead it is proposed to use approximate energy methods, coupling together FE and classical solutions with models of the contained fluid to study vibrations at low to medium frequencies (50–500 Hz, say). As a precursor to this long term project an initial review of the limitations of classical and FE methods is necessary and this forms the motivation for the present work.

With this in mind, the paper proceeds from a recapitulation of thin shell assumptions to an improved theory in some detail. Three different theories are presented and applied to a cylindrical pipe and a series of shells evolving from a flat plate to an open circular cylindrical shell, subjected to simply supported boundary conditions. The corresponding FE models are then constructed to provide numerical solutions. An appraisal of the three theories is achieved by comparing the analytical solutions and FE results, leading to some comments and conclusions about the accuracy of the FE models.

2. CLASSICAL ANALYSIS

Theories concerning shells abound, since simplifying approximations can be made at various points in the derivation of the governing equations (see, for example, Chapter 1 of the book by Leissa [1] and Calladine [2]). One of the simpler theories for thin shells is that of Love [3]. Some represent a further simplification of the derivation of the thin shell equations as proposed by Love (e.g., the theory of Donnell [4]). Others represent so called "first order" theories, in which one or more of Love's postulates are relaxed and the first-order transverse shear deformation and rotary inertia are incorporated to allow for arbitrary rotations of normals to the midsurface. These can be applied to moderately thick shells, as in the case of the Flügge–Lur'ye–Byrne theory [5–7] in which the thin shell approximation is retained whilst the shell's thinness is assumed proportional to $(h/a)^2 \ll 1$ as opposed to $h/a \ll 1$. Finally, there are so-called "higher order" theories, which generalize "first order" theories by eliminating dependence on the shear correction factor; they are, therefore, valid for a relatively thick shell. Most of the higher order theories assume cubic inplane displacements in the through thickness direction, and transverse inextensibility. Here a comparison is made of the theories of Donnell [4] and Love [3] (but using as a basis the Reissner–Naghdi–Berry [8, 9] version of Love's theory) and an improved theory (first order) which includes the effects of rotary inertia and transverse shear and which can be attributed to various workers in the field (see for example reference [10] and the references therein).

Pipes of fairly small thickness to radius ratio, $h/a \leqslant 0{\cdot}1$, are the primary subject of interest here, with a being the radius and h the thickness of the shell. Such thin-walled pipes admit the use of thin shell theories and first order theory and allow the equations of motion to be described in terms of the deformation of a reference surface, which here is taken to be the middle surface of the pipe. In addition, the comparison is restricted to pipes of constant thickness and uniform properties, ignoring temperature gradients.

2.1. Love's first approximation

Thin shell theories typically include the postulates expressed in Love's first approximation [3] as a common basis. These postulates may be written as follows: (i) the thickness of a shell is small compared to a characteristic dimension; (ii) the deflections of the shell are small; (iii) the transverse normal stress is negligible and (iv) normals to the reference surface of the shell remain normals and the shell thickness remains unchanged.

Postulate (i) presents the general definition of a thin shell. Generally, the characteristic dimension is the radius of curvature or the shortest planform dimension. For vibration analysis, the wavelength of the transverse displacement can be the characteristic dimension. Here a shell is taken to be thin if the ratio of its thickness to the radius of the curvature of its surface is less than or approximately equal to one-tenth, $h/a \leqslant 0{\cdot}1$. Postulate (ii) permits the use of the equations of the undeformed shell to describe its subsequent deformation and, with the use of Hooke's law, results in a linear elastic theory. Postulate (iii) is a result of postulate (i). The first part of the fourth postulate, that of the preservation of the normal, represents an extension of Euler–Bernoulli beam theory to the problem of transverse bending in shells and requires that locally plane sections remain plane during deformations of the shell. The second part requires that all the strain components in the direction normal to the reference surface vanish.

Love's postulates imply that a generic point in the volume of a shell can be described in terms of the behaviour of a point on a reference surface of the shell, which is taken to be the middle surface for convenience. This process reduces the problem from a full three-dimensional treatment of the shell to a two-dimensional one. For ease of derivation, the shell geometry is described in terms of the orthogonal set of curvilinear coordinates which correspond to the orthogonal lines of principal curvature. Relationships describing the differential geometry of the shell can be found in references [11, 12].

Hooke's law for a homogeneous elastic medium is expressed in terms of the principal coordinates of the shell. By Love's postulate (iii) it is assumed that the transverse normal stress is zero and that by postulate (iv) the transverse normal strain and the transverse shearing strains are also zero, further simplifying the analysis. The shell displacements can be related to the strains by linear theory [11]. In Love's theory the fourth postulate is invoked when deriving the stress–strain relations: it is assumed that the displacements are linearly distributed through the thickness of the shell. The thin-shell approximation is then introduced to simplify the resulting non-vanishing strains in terms of the displacements (higher order theories generally diverge from Love's theory at this stage).

2.2. DERIVATION OF THE EQUATIONS OF MOTION

The derivation of the equations of motion is summarized here. A more detailed derivation can be found in many texts on shells [1, 10–12]. Figure 1 indicates the system of coordinates used in this case: axial coordinate x, radial coordinate r, azimuthal coordinate θ and displacements in the coordinate directions u_x, w and u_θ respectively, as well as rotations β_x and β_θ. For convenience these have been made dimensionless as follows: $\bar{u}_x = u_x/a$, $\bar{w} = w/a$ and $\bar{u}_\theta = u_\theta/a$, where we recall that a is the radius of the mid surface or reference surface of the shell. The variable x is made dimensionless using $\eta = x/a$. The variable ζ is defined to be the perpendicular distance from the reference surface ($-h/2 \leqslant \zeta \leqslant h/2$). The strain–displacement relations for a circular cylindrical shell are then given by

$$\varepsilon_x = \varepsilon_x^0 + \zeta\kappa_x, \qquad \varepsilon_\theta = \varepsilon_\theta^0 + \zeta\kappa_\theta, \qquad \gamma_{x\theta} = \gamma_{x\theta}^0 + \zeta\tau, \tag{1}$$

where ε_x, ε_θ and $\gamma_{x\theta}$ represent the in-plane strains and shearing strains; κ_x and κ_θ are the bending components of the strain representing changes in the curvature of the reference surface during deformation; and τ is the torsion of the reference

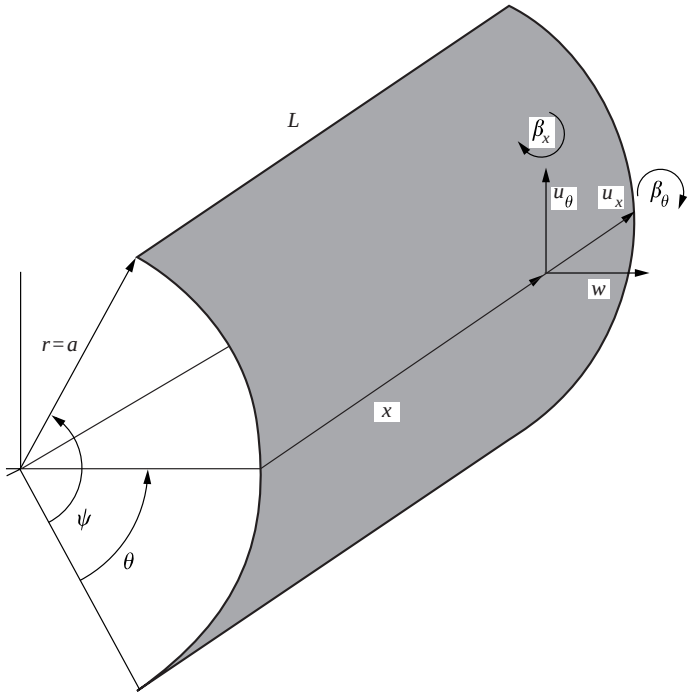

Figure 1. Coordinates for a cylindrical shell.

surface during deformation. Terms with superscripts zero represent the normal and shearing strains on the reference surface. These various terms are given by

$$\varepsilon_x^0 = \frac{\partial \bar{u}_x}{\partial \eta}, \qquad \varepsilon_\theta^0 = \frac{\partial \bar{u}_\theta}{\partial \theta} + \bar{w},$$

$$\kappa_x = \frac{1}{a}\frac{\partial \beta_x}{\partial \eta}, \qquad \kappa_\theta = \frac{1}{a}\frac{\partial \beta_\theta}{\partial \theta},$$

$$\gamma_{x\theta}^0 = \frac{\partial \bar{u}_\theta}{\partial \eta} + \frac{\partial \bar{u}_x}{\partial \theta}, \qquad \tau = \frac{1}{a}\left(\frac{\partial \beta_\theta}{\partial \eta} + \frac{\partial \beta_x}{\partial \theta}\right), \tag{2}$$

while the rotations of the tangents to the reference surface, β_x and β_θ (see Figure 1) are given by (except for the improved theory, discussed below)

$$\beta_x = -\frac{\partial \bar{w}}{\partial \eta}, \qquad \beta_\theta = \bar{u}_\theta - \frac{\partial \bar{w}}{\partial \theta}. \tag{3}$$

The equivalent static stress resultants, obtained from the integration of the stresses across the thickness of the shell (which is assumed to be isotropic), are given by Hooke's law:

$$N_x = K(\varepsilon_x^0 + \varepsilon_\theta^0 \nu), \qquad N_\theta = K(\varepsilon_\theta^0 + \varepsilon_x^0 \nu), \qquad N_{x\theta} = N_{\theta x} = Gh\gamma_{x\theta}^0. \tag{4}$$

The equivalent static couples are given in these theories by:

$$M_x = D(\kappa_x + \kappa_\theta \nu), \qquad M_\theta = D(\kappa_\theta + \kappa_x \nu), \qquad M_{x\theta} = M_{\theta x} = K_0 D\tau = Gh^3\tau/12, \tag{5}$$

where ν, G and E are, respectively, Poisson's ratio, the shear modulus, and Young's modulus for the material; $K_0 = (1 - \nu)/2$; and K and D are the extensional and the bending rigidity of the shell, given by $K = Eh/(1 - \nu^2)$, $D = Eh^3/12(1 - \nu^2)$. The equations of motion can then be obtained from Hamilton's principle, leading to

$$\frac{\partial N_x}{\partial \eta} + \frac{\partial N_{\theta x}}{\partial \theta} = a^2 \rho h \ddot{\bar{u}}_x, \qquad \frac{\partial N_\theta}{\partial \theta} + \frac{\partial N_{x\theta}}{\partial \eta} + Q_\theta = a^2 \rho h \ddot{\bar{u}}_\theta,$$

$$\frac{\partial Q_x}{\partial \eta} + \frac{\partial Q_\theta}{\partial \theta} - N_\theta = a^2 \rho h \ddot{\bar{w}} + q_n,$$

$$\frac{\partial M_x}{\partial \eta} + \frac{\partial M_{\theta x}}{\partial \theta} - aQ_x = 0, \qquad \frac{\partial M_{x\theta}}{\partial \eta} + \frac{\partial M_\theta}{\partial \theta} - aQ_\theta = 0, \tag{6}$$

where q_n represents the external forces acting normal to the surface of the shell and ρ is the density of the shell material. The last two lines of equation (6) give the equivalent static shearing stresses Q_x and Q_θ enabling them to be eliminated from the equations of motion. Note that this is not the case for the improved theory.

2.2.1. *Love's theory*

Substituting equations (4) and (5) into equation (6) yields the equations of motion for Love's theory:

$$\frac{\partial^2 \bar{u}_x}{\partial \eta^2} + K_0 \frac{\partial^2 \bar{u}_x}{\partial \theta^2} + K_0' \frac{\partial^2 \bar{u}_\theta}{\partial \theta \partial \eta} + \nu \frac{\partial \bar{w}}{\partial \eta} = \frac{a^2}{c_p^2} \ddot{\bar{u}}_x,$$

$$K_0' \frac{\partial^2 \bar{u}_x}{\partial \theta \partial \eta} + (1+\varepsilon) K_0 \frac{\partial^2 \bar{u}_\theta}{\partial \eta^2} + (1+\varepsilon) \frac{\partial^2 \bar{u}_\theta}{\partial \theta^2} + \frac{\partial \bar{w}}{\partial \theta} - \varepsilon \left(\frac{\partial^3 \bar{w}}{\partial \theta^3} + \frac{\partial^3 \bar{w}}{\partial \theta^2 \partial \eta} \right) = \frac{a^2}{c_p^2} \ddot{\bar{u}}_\theta,$$

$$-\nu \frac{\partial \bar{u}_x}{\partial \eta} - \frac{\partial \bar{u}_\theta}{\partial \theta} + \varepsilon \left(\frac{\partial^3 \bar{u}_\theta}{\partial \theta^3} + \frac{\partial^3 \bar{u}_\theta}{\partial \eta^2 \partial \theta} \right) - \varepsilon \nabla_{\eta\theta}^4 \bar{w} - \bar{w} = \frac{a^2}{c_p^2} \ddot{\bar{w}} + \frac{a q_n}{K}, \tag{7}$$

where $\nabla_{\eta\theta}^2 = \partial^2/\partial\eta^2 + \partial^2/\partial\theta^2$, $\varepsilon = h^2/(12a^2)$, $K_0' = (1+\nu)/2$, and $c_p^2 = E/[\,\rho(1-\nu^2)]$ (c_p is the phase speed of a flexural wave propagating in a thin plate).

2.2.2. *Donnell's theory*

Donnell's theory [4, 10] represents a further simplification of the theory of Love and is applicable in the case of sufficiently thin shells. It is appropriate only for responses with large numbers of circumferential waves, especially for long cylindrical shells. It is argued that in the equations of motion (6) the transverse shearing stress resultant Q_θ makes a negligible contribution to the equilibrium forces in the circumferential direction, and hence Q_θ may be neglected in the second line of equation (6). Secondly it is argued that the stretching displacement u_θ has no effect on the relationship between curvature and the displacements. The curvatures expressed in equation (2) are therefore altered as follows

$$\kappa_x = -\frac{1}{a} \frac{\partial^2 \bar{w}}{\partial \eta^2}, \qquad \kappa_\theta = -\frac{1}{a} \frac{\partial^2 \bar{w}}{\partial \theta^2}, \qquad \tau = -\frac{2}{a} \frac{\partial^2 \bar{w}}{\partial \theta \partial \eta}. \tag{8}$$

Clearly this has an effect on the resulting couples as expressed by equation (5), and upon substitution the equations of motion for a cylindrical shell become

$$\frac{\partial^2 \bar{u}_x}{\partial \eta^2} + K_0 \frac{\partial^2 \bar{u}_x}{\partial \theta^2} + K_0' \frac{\partial^2 \bar{u}_\theta}{\partial \theta \partial \eta} + \nu \frac{\partial \bar{w}}{\partial \eta} = \frac{a^2}{c_p^2} \ddot{\bar{u}}_x,$$

$$K_0' \frac{\partial^2 \bar{u}_x}{\partial \theta \partial \eta} + K_0 \frac{\partial^2 \bar{u}_\theta}{\partial \eta^2} + \frac{\partial^2 \bar{u}_\theta}{\partial \theta^2} + \frac{\partial \bar{w}}{\partial \theta} = \frac{a^2}{c_p^2} \ddot{\bar{u}}_\theta,$$

$$-\nu \frac{\partial \bar{u}_x}{\partial \eta} - \frac{\partial \bar{u}_\theta}{\partial \theta} - \varepsilon \nabla_{\eta\theta}^4 \bar{w} - \bar{w} = \frac{a^2}{c_p^2} \ddot{\bar{w}} + \frac{a q_n}{K}. \tag{9}$$

These two assumptions lead to treating a thin shell of small curvature as if it were a thin plate. The resulting equations differ very little from the membrane equations of a shell [12, 13], except for the term $\varepsilon \nabla_{\eta\theta}^4 \bar{w}$ in the last line. This term arises from the transverse forces Q_θ and Q_x.

2.2.3. *Improved theory*

Next an improved theory for circular cylindrical shells is considered which includes the effect of rotary inertia and transverse shear [10]. A full derivation of the equations of motion in this case can be found in references [10–12]. The derivation proceeds in a similar fashion to that for Love's theory except that fewer assumptions are made.

Firstly, Love's postulate (iv), that normals to the reference surface of the shell remain normals and the shell thickness undergoes no change in length during the deformation, is partly relaxed; i.e., normals to the reference surface of the shell no longer remain normal, but they remain straight during deformation. This allows rotations of normals to the midsurface, and the two associated variables β_x and β_θ are thus independent [equation (3) is abandoned]. Hence the number of independent variables is increased to five, namely, $\bar{u}_x$, $\bar{u}_\theta$, $\bar{w}$, β_x and β_θ. In this way the theory is extended to include the first-order transverse shear deformation. Accordingly, the transverse forces Q_x and Q_θ are not eliminated from the equations of motion as in equation (6), but are replaced by expressions derived independently. The effects of rotary inertia are also included in the improved theory.

Finally, this theory includes terms of higher order in ζ/a when the stresses are integrated over the thickness of the shell [the strain–displacement relationships, e.g., ε_θ, involve the Lamé parameter, $1/(1+\zeta/a)$, which is approximated by unity in thin shell theory, c.f. equation (1)]. Terms of higher order than third, however, are neglected. The other assumptions remain in place. Postulate (ii) requires that the deformations be small: this is essential if a linear theory is required. The full derivation yields the following set of governing differential equations:

$$\frac{\partial^2 \bar{u}_x}{\partial \eta^2} + K_0(1+\varepsilon)\frac{\partial^2 \bar{u}_x}{\partial \theta^2} + K_0'\frac{\partial^2 \bar{u}_\theta}{\partial \eta \partial \theta} + \nu\frac{\partial \bar{w}}{\partial \eta} + \varepsilon\left(\frac{\partial^2 \beta_x}{\partial \eta^2} - K_0\frac{\partial^2 \beta_x}{\partial \theta^2}\right) = \frac{a^2}{c_p^2}(\ddot{\bar{u}}_x + \varepsilon\ddot{\beta}_x), \tag{10a}$$

$$K_0'\frac{\partial^2 \bar{u}_x}{\partial \eta \partial \theta} - k_0 K_0 \bar{u}_\theta + K_0\frac{\partial^2 \bar{u}_\theta}{\partial \eta^2} + (1+\varepsilon)\frac{\partial^2 \bar{u}_\theta}{\partial \theta^2} + (1+\varepsilon+k_0K_0)\frac{\partial \bar{w}}{\partial \theta}$$

$$+ k_0 K_0 \beta_\theta + \varepsilon\left(K_0\frac{\partial^2 \beta_\theta}{\partial \eta^2} - \frac{\partial^2 \beta_\theta}{\partial \theta^2}\right) = \frac{a^2}{c_p^2}(\ddot{\bar{u}}_\theta + \varepsilon\ddot{\beta}_\theta), \tag{10b}$$

$$-\nu\frac{\partial \bar{u}_x}{\partial \eta} - (1+\varepsilon+k_0K_0)\frac{\partial \bar{u}_\theta}{\partial \theta} + k_0K_0\left(\frac{\partial^2 \bar{w}}{\partial \eta^2} + \frac{\partial^2 \bar{w}}{\partial \theta^2}\right)$$

$$-(1+\varepsilon)\bar{w} + k_0K_0\frac{\partial \beta_x}{\partial \eta} + (k_0K_0+\varepsilon)\frac{\partial \beta_\theta}{\partial \theta} = \frac{a^2}{c_p^2}\ddot{\bar{w}} + \frac{aq_n}{K}, \tag{10c}$$

$$\varepsilon\left(\frac{\partial^2 \bar{u}_x}{\partial \eta^2} - K_0 \frac{\partial^2 \bar{u}_x}{\partial \theta^2}\right) - k_0 K_0 \frac{\partial \bar{w}}{\partial \eta} + \varepsilon\left(\frac{\partial^2 \beta_x}{\partial \eta^2} + K_0 \frac{\partial^2 \beta_x}{\partial \theta^2}\right)$$

$$- k_0 K_0 \beta_x + \varepsilon K_0' \frac{\partial^2 \beta_\theta}{\partial \eta \partial \theta} = \frac{a^2 \varepsilon}{c_p^2} (\ddot{\bar{u}}_x + \ddot{\beta}_x), \tag{10d}$$

$$k_0 K_0 \bar{u}_\theta + \varepsilon\left(K_0 \frac{\partial^2 \bar{u}_\theta}{\partial \eta^2} - \frac{\partial^2 \bar{u}_\theta}{\partial \theta^2}\right) - (k_0 K_0 + \varepsilon) \frac{\partial \bar{w}}{\partial \theta}$$

$$+ \varepsilon\left(K_0' \frac{\partial^2 \beta_x}{\partial \eta \partial \theta} + K_0 \frac{\partial^2 \beta_\theta}{\partial \eta^2} + \frac{\partial^2 \beta_\theta}{\partial \theta^2}\right) - k_0 K_0 \beta_\theta = \frac{a^2 \varepsilon}{c_p^2} (\ddot{\bar{u}}_\theta + \ddot{\beta}_\theta), \tag{10e}$$

where k_0 is a shearing correction coefficient and the other constants are as previously defined for Love's theory.

2.2.4. *Boundary conditions*

In the case of the improved theory it is necessary to specify five boundary conditions for each edge, one from each of the following five pairs:

$$N_n \quad \text{or} \quad u_n', \qquad N_{ns} \quad \text{or} \quad u_s',$$
$$Q_n \quad \text{or} \quad w', \qquad M_n \quad \text{or} \quad \beta_n', \qquad M_{ns} \quad \text{or} \quad \beta_s'. \tag{11}$$

Here the subscript n denotes the component normal to the edge, while s denotes the component parallel to the edge. In the case of Love's or Donnell's theory, only four of these boundary conditions need be specified, since it can be shown that these five boundary conditions do not form an independent set in these cases but can be re-expressed in terms of Kirchhoff's effective shearing stresses [10, 11] [see, for example, equations (12a)].

2.3. APPLICATION TO SIMPLY SUPPORTED PIPES

Equations (7), (9) and (10) are next solved for an example pipe, in order to establish whether any notable differences exist between the theories for typical pipe parameters. We consider a pipe of length L, radius a and thickness h simply supported at both ends with no normal constraints (see Figure 1).

2.3.1. *Boundary conditions*

The boundary conditions appropriate to Love's theory and Donnell's theory for such a pipe are

$$N_x = 0, \qquad \bar{u}_\theta = 0, \qquad \bar{w} = 0, \qquad M_x = 0, \tag{12a}$$

at $\eta = 0$ and $\eta = L/a$, i.e., the ends are free to translate in the axial direction and are not subjected to bending moments. In addition to these, the condition on shear deformation leads to

$$\beta_\theta = 0 \tag{12b}$$

at $\eta = 0$ and $\eta = L/a$ for the improved theory.

2.3.2. *Normal mode shapes*

The set of normal modes which satisfy the boundary conditions for Love's and Donnell's theory is given by

$$\bar{u}_x = -\sum_{m=1}^{\infty}\sum_{n=0}^{\infty}\sum_{l=0}^{1} A_{1mnl}\cos(\beta_m\eta)\Theta_l(n\theta)\,\mathrm{e}^{\mathrm{i}\omega_{nm}t},$$

$$\bar{u}_\theta = \sum_{m=1}^{\infty}\sum_{n=0}^{\infty}\sum_{l=0}^{1} A_{2mnl}\sin(\beta_m\eta)\Theta_l(n\theta+\pi/2)\,\mathrm{e}^{\mathrm{i}\omega_{nm}t},$$

$$\bar{w} = \sum_{m=1}^{\infty}\sum_{n=0}^{\infty}\sum_{l=0}^{1} A_{3mnl}\sin(\beta_m\eta)\Theta_l(n\theta)\,\mathrm{e}^{\mathrm{i}\omega_{nm}t}, \tag{13a}$$

where m and n are the axial and circumferential mode numbers, respectively. In addition, for the improved theory,

$$\beta_x = -\sum_{m=1}^{\infty}\sum_{n=0}^{\infty}\sum_{l=0}^{1} A_{4mnl}\cos(\beta_m\eta)\Theta_l(n\theta)\,\mathrm{e}^{\mathrm{i}\omega_{nm}t},$$

$$\beta_\theta = \sum_{m=1}^{\infty}\sum_{n=0}^{\infty}\sum_{l=0}^{1} A_{5mnl}\sin(\beta_m\eta)\Theta_l(n\theta+\pi/2)\,\mathrm{e}^{\mathrm{i}\omega_{nm}t}, \tag{13b}$$

where

$$\beta_m = (m\pi a)/L, \qquad \Theta_l(n\theta) = \sin(n\theta + l\pi/2), \qquad l = 0, 1. \tag{13c}$$

These equations give rise to pairs of modes ($l = 0, 1$) shifted by $\theta = \pi/2$ (except for $n = 0$); i.e., $A_{imn1} = A_{imn0} = A_{imn}$, and the corresponding frequencies occur in pairs.

2.3.3. *Natural frequencies*

The natural frequencies can be extracted by solving the determinants acquired from the differential equations using the assumed normal modes. The natural frequencies for Love's, Donnell's, and the improved theory are denoted by ω^L_{nm}, ω^D_{nm}, and ω^I_{nm}, respectively.

In the case of Love's theory, the natural frequencies of the torsional modes ($\bar{u}_x = 0$ and $\bar{w} = 0$) are given by

$$\omega^L_{nm} = \frac{c_p}{a}\sqrt{(1+\varepsilon)K_0}\beta_m, \tag{14}$$

while the longitudinal and radial or ring modes, for which $\bar{u}_\theta = 0$, are given by the solution of the quadratic in $\omega^{L^2}_{nm}$,

$$\frac{a^4}{c_p^4}\omega^{L^4}_{nm} - (1+(1+\varepsilon\beta_m^2)\beta_m^2)\frac{a^2}{c_p^2}\omega^{L^2}_{nm} + (1-\nu^2)\beta_m^2 + \varepsilon\beta_m^6 = 0. \tag{15}$$

This has two positive roots, one coresponding to the longitudinal mode and the other to the radial or ring mode. Similarly, the natural frequencies of the torsional modes obtained from Donnell's theory are

$$\omega_{nm}^{D} = \frac{c_p}{a}\sqrt{K_0}\beta_m. \tag{16}$$

It can be shown by decomposing the determinant that the natural frequencies of the other (longitudinal and ring) axisymmetric ($n = 0$) modes are also given in Donnell's theory by the solution of equation (15). Thus Donnell's and Love's theories return the same natural frequencies for the radial and longitudinal axisymmetric modes (though not for $n > 0$). For the improved theory, use of equations (13a) and (13b) leads to a 5×5 determinant which must be set to zero to obtain the natural frequencies ω_{nm}^{I}. The determinant can be decomposed into 2×2 and 3×3 determinants for convenience, from which, respectively, the natural frequencies of the torsional modes ($\bar{u}_x = 0, \bar{w} = 0, \beta_x = 0$) and the axisymmetric modes ($\bar{u}_\theta = 0, \beta_\theta = 0$) can be obtained.

The 2×2 determinant satisfies

$$|d_{ij}| = 0, \qquad i, j = 1, 2, \tag{17a}$$

with

$$d_{11} = -\frac{a^2}{c_p^2}\omega_{nm}^2 + k_0K_0 + K_0\beta_m^2,$$

$$d_{12} = d_{21} = \varepsilon\left(\frac{a^2}{c_p^2}\omega_{nm}^2 + K_0\beta_m^2\right) - k_0K_0,$$

$$d_{22} = \varepsilon\left(K_0'\beta_m^2 + \frac{a^2}{c_p^2}\omega_{nm}^2\right) - k_0K_0. \tag{17b}$$

The 3×3 determinant satisfies

$$|e_{ij}| = 0, \qquad i, j = 1, 2, 3, \tag{18a}$$

with

$$e_{11} = \beta_m^2 - \frac{a^2}{c_p^2}\omega_{nm}^2, \qquad e_{12} = e_{21} = \nu\beta_m,$$

$$e_{13} = e_{31} = \varepsilon\left(\beta_m^2 - \frac{a^2}{c_p^2}\omega_{nm}^2\right), \qquad e_{22} = \frac{a^2}{c_p^2}\omega_{nm}^2 + k_0K_0\beta_m^2 + 1 + \varepsilon,$$

$$e_{23} = e_{32} = -k_0K_0\beta_m, \qquad e_{33} = \varepsilon\left(\beta_m^2 - \frac{a^2}{c_p^2}\omega_{nm}^2\right) + k_0K_0. \tag{18b}$$

The equation with the 3×3 determinant can be solved by root searching to obtain the ω_{nm}^{I}. Using the natural frequencies, one may then solve for each A_{inm}, in terms of A_{1nm}, to obtain each of the modal displacements by means of equations (13).

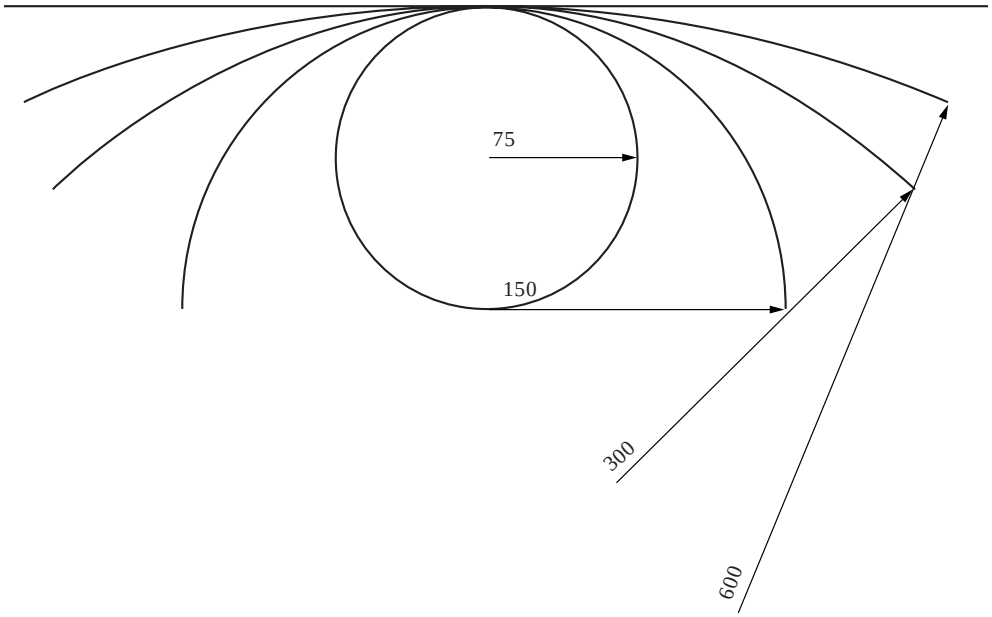

Figure 2. Schematic of open shells evolving from a plate ($\psi = 0$) to a pipe with slit ($\psi = 2\pi$).

2.4. APPLICATION TO SIMPLY SUPPORTED OPEN CYLINDRICAL SHELLS

We have also compared results from classical analysis with finite element results for open cylindrical shells. Here we review the theories. Consider an open shell of length L, radius b, thickness h and opening angle ψ simply supported with no normal constraints at each end and also simply supported on the open edges. We define a length a, which is the radius of the equivalent closed pipe whose circumference is L_c, i.e., $L_c = 2\pi a = \psi b$.

2.4.1. *Boundary conditions*

The boundary conditions at $\eta = 0$ and $\eta = L/a$ are as before, but in addition there are boundary conditions on each straight edge given by

$$\bar{u}_x = 0, \qquad N_\theta = 0, \qquad \bar{w} = 0, \qquad M_\theta = 0, \tag{19a}$$

TABLE 1

Models used for comparison of the thin shell theories and FE analyses

Structure	b/a	Opening angle ψ	Ring frequency
Pipe	1	Closed	11·4 kHz
Open shell	1	2π	11·4 kHz
	2	π	5·70 kHz
	4	$\pi/2$	2·85 kHz
	8	$\pi/4$	1·43 kHz
	180	$\pi/90$	63 kHz
Flat plate	∞	0	0

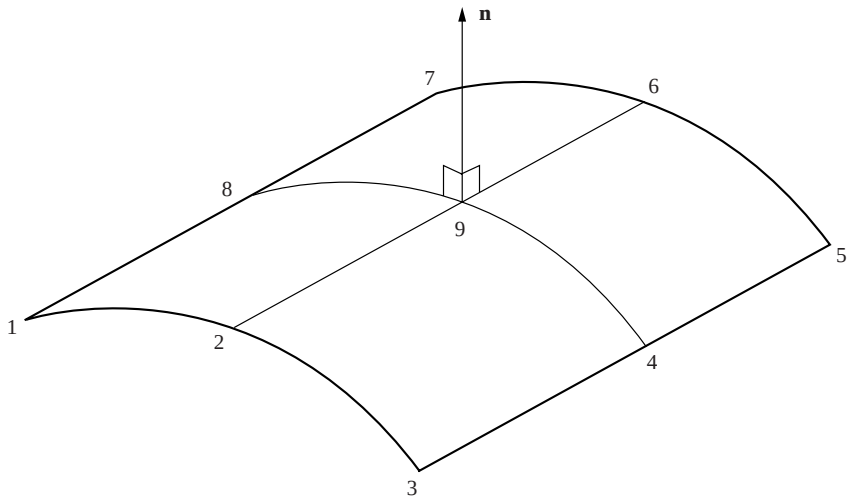

Figure 3. Quadrilateral parabolic shell element with 9 nodes.

at $\theta = 0$ and $\theta = \psi$, i.e., the edges are not free to translate in the axial and radial directions, but are free to translate in the circumferential direction, without bending moments being applied to them. In addition to these, for the improved theory

$$\beta_x = 0 \tag{19b}$$

at $\theta = 0$ and $\theta = \psi$.

2.4.2. *Normal mode shapes*

The set of normal modes which satisfy the boundary conditions for Love's and Donnell's theory is now given by

$$\bar{u}_x = -\sum_{m=1}^{\infty}\sum_{n=0}^{\infty} A_{1mn} \cos(\beta_m \eta) \sin(\beta_n \theta)\, e^{i\omega_{nm} t},$$

$$\bar{u}_\theta = \sum_{m=1}^{\infty}\sum_{n=0}^{\infty} A_{2mn} \sin(\beta_m \eta) \cos(\beta_n \theta)\, e^{i\omega_{nm} t},$$

$$\bar{w} = \sum_{m=1}^{\infty}\sum_{n=0}^{\infty} A_{3mn} \sin(\beta_m \eta) \sin(\beta_n \theta)\, e^{i\omega_{nm} t}, \tag{20a}$$

where m and n are again the axial and circumferential mode numbers, respectively. In addition, for the improved theory,

$$\beta_x = -\sum_{m=1}^{\infty}\sum_{n=0}^{\infty} A_{4mn} \cos(\beta_m \eta) \sin(\beta_n \theta)\, e^{i\omega_{nm} t},$$

$$\beta_\theta = \sum_{m=1}^{\infty}\sum_{n=0}^{\infty} A_{5mn} \sin(\beta_m \eta) \cos(\beta_n \theta)\, e^{i\omega_{nm} t}, \tag{20b}$$

TABLE 2

Comparison of natural frequencies for analytical and numerical pipe models

n	m	Donnell (Hz)	Love (Hz)	Improved (Hz)	FE(r) (900) (Hz)	FE (900) (Hz)	FE (3148) (Hz)	FE(A) (900) (Hz)
0 (torsional)	1	533·60	533·69	533·79	533·61	533·75	533·80	533·74
0 (torsional)	2	1067·2	1067·4	1067·6	1067·2	1067·4	1067·6	1067·5
0 (torsional)	3	1607·8	1601·1	1601·4	1600·4	1600·9	1601·3	1601·2
0 (longitudinal)	1	856·86	856·86	856·94	856·81	856·81	856·84	856·88
0 (longitudinal)	2	1712·3	1712·3	1713·0	1719·6	1712·0	1709·3	1712·4
1	1	162·74	47·755	47·184	47·659	47·200	47·203	47·200
1	2	242·43	184·980	184·17	184·69	184·23	184·24	184·23
1	3	433·30	399·73	399·01	399·60	399·13	399·16	399·13
2	1	786·18	589·74	588·69	588·33	588·43	588·07	590·31
2	2	791·37	595·57	594·07	593·13	593·51	593·11	595·43
2	3	805·38	612·32	610·97	608·29	609·11	608·68	611·09
3	1	1874·6	1665·6	1659·5	1657·3	1657·3	1655·3	1658·6
3	2	1878·3	1669·3	1662·9	1663·1	1660·6	1664·6	1667·3
3	3	1885·1	1676·1	1669·3	1671·6	1666·6	1670·3	1675·4

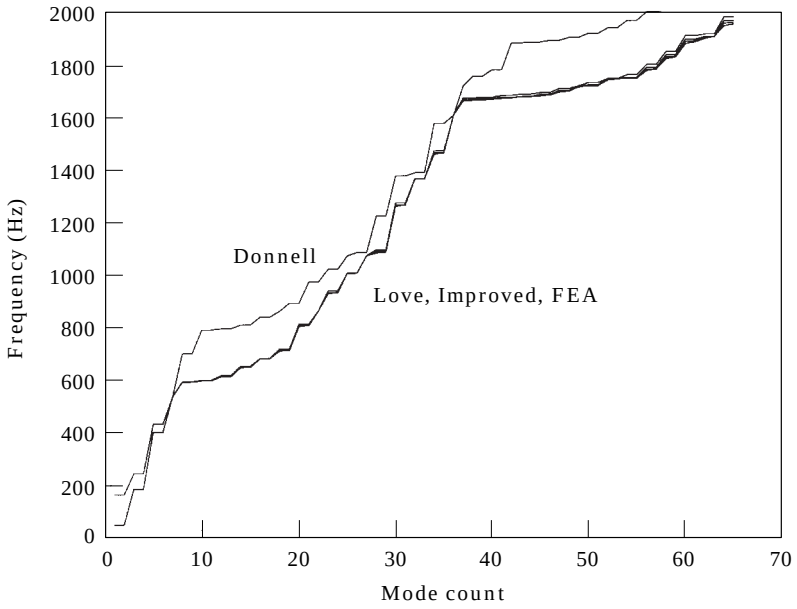

Figure 4. Mode count for pipe models.

where

$$\beta_m = \frac{m\pi b}{L}, \qquad \beta_n = \frac{n\pi}{\psi}. \tag{20c}$$

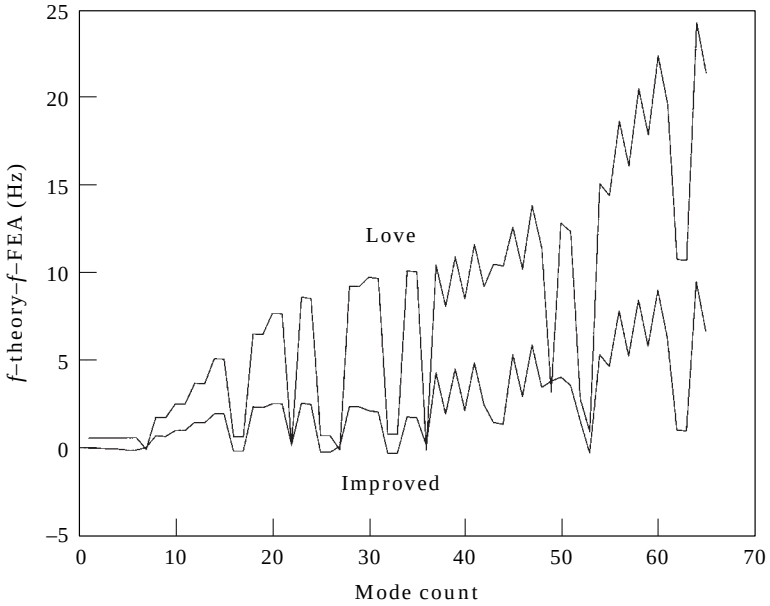

Figure 5. Deviation of Improved and Love's theory from FE model.

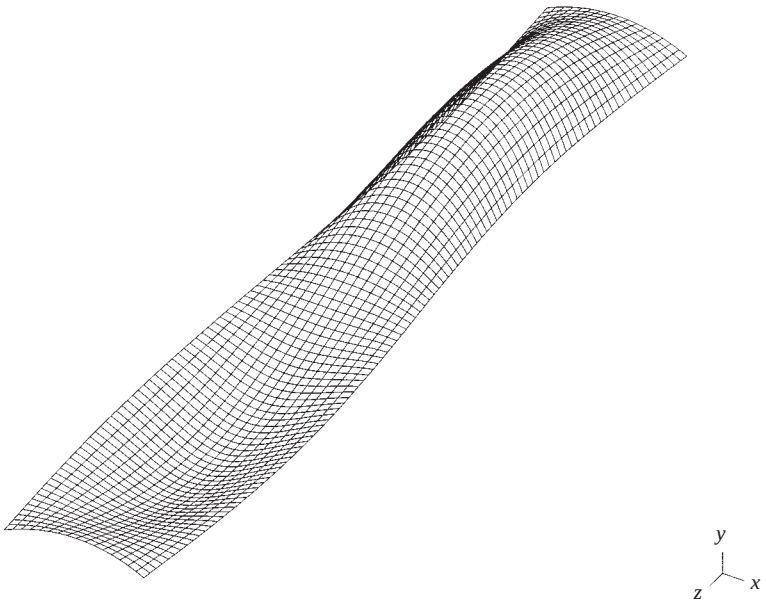

Figure 6. Deformed FE mesh (900 meshes) for $m = 2$, $n = 1$ mode.

Substitution of these mode shapes into the governing differential equations yields determinants similar to those for the pipe, from which the natural frequencies and modes may be obtained. In this case, axisymmetric radial and longitudinal modes (ring modes), for which $\bar{u}_\theta = 0$ and $n = 0$, are not permitted by the boundary conditions. The only modes associated with $n = 0$ which occur in this case are the torsional modes. It is, however, convenient to define "ring frequencies", corresponding to an open shell with free boundary conditions at edges $\theta = 0$ and $\theta = \psi$ [cf. equations (19a) but now the radial translation is allowed]. Such ring frequencies are therefore equal to those for a cylindrical pipe of the same radius of curvature. They are used below in discussing the types of behaviour observed in open shells.

3. RESULTS: COMPARISON WITH FINITE ELEMENT ANALYSIS

In order to compare results from the various theories outlined above with those from finite element (FE) analysis, a model has been constructed for a pipe which might be considered typical of water-main runs on many offshore installations and structures. Models have also been constructed for various open singly curved shells (gutters) of differing radii of curvature, but the same length, surface area and thickness as the pipe models. Using open shell models in this way, it is possible to isolate the effects that shell curvature has upon the respective natural frequencies of the models. The FE models were typically constructed with 900 elements (12 circumferential by 75 longitudinal elements). However, in order to examine convergence of the FE analysis, a larger 3148 element mesh was also used for the pipe model. The FE analysis utilized the commercial IDEAS software package [16] and ABAQUS [17].

3.1. MODEL PARAMETERS

3.1.1. *Pipe model*

The pipe model has the following dimensions: length $L = 3{\cdot}0$ m, diameter $2a = 0{\cdot}15$ m, and wall thickness $h = 0{\cdot}005$ m; and the material properties of steel: Young's modulus $E = 206{\cdot}8 \times 10^9$ Pa, Poisson's ratio $\nu = 0{\cdot}29$, shear modulus $G = 80{\cdot}16 \times 10^9$ Pa, density $\rho = 7{\cdot}82 \times 10^3$ kg. As has already been noted, these parameters are representative of typical water-main pipe runs on many offshore structures.

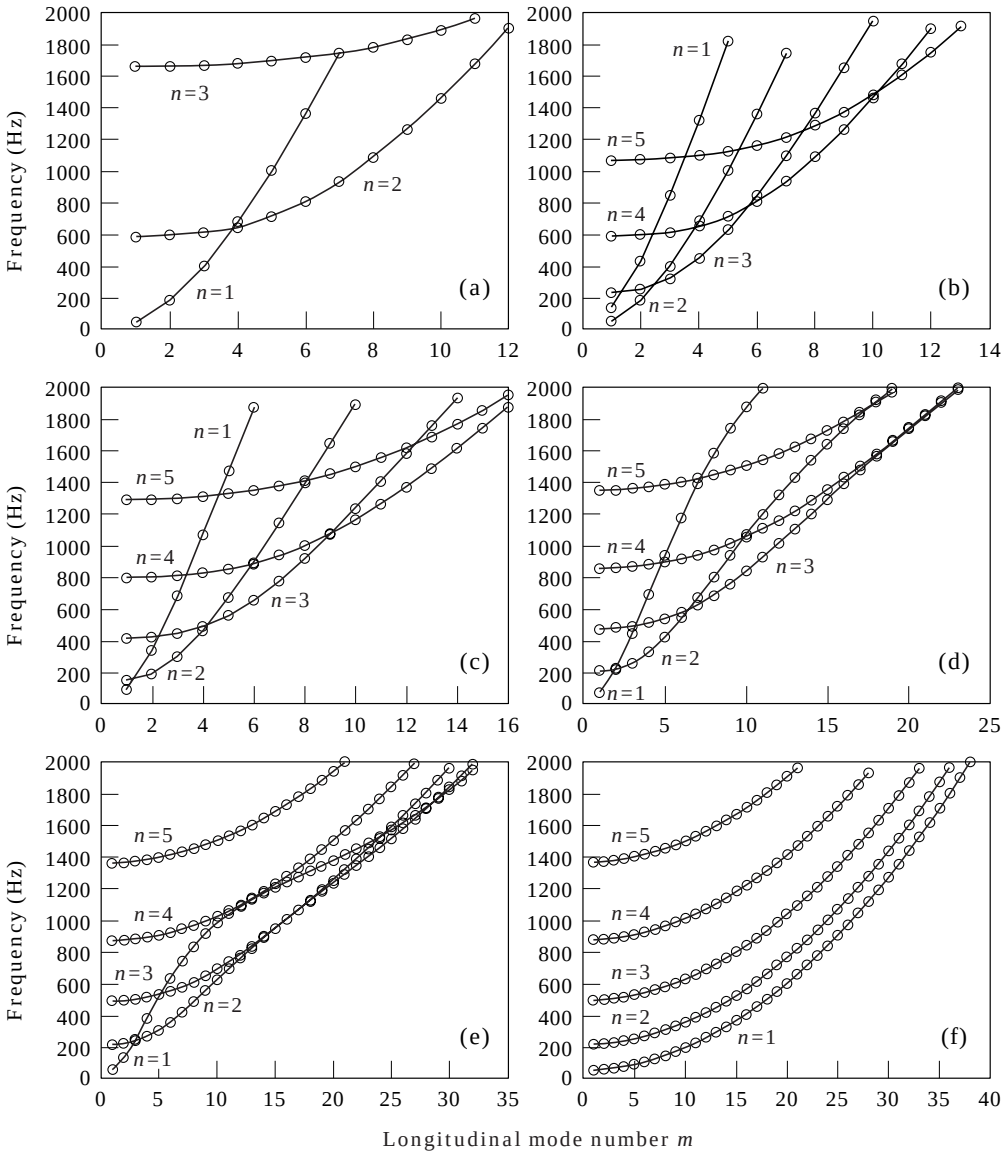

Figure 7. Modal frequencies based on the improved theory for a pipe and for open shells: (a) Pipe; (b) $\psi = 2\pi$; (c) $\psi = \pi$; (d) $\psi = \pi/2$; (e) $\psi = \pi/4$; (f) $\psi = \pi/90$.

3.1.2. *Open shell models of different radii of curvature*

The open shell models evolving from a plate to an open circular cylindrical shell have the following dimensions (see Figure 2): length $L = 3{\cdot}0$ m, radii of curvature b defined by ψ, lengths of curved side $L_c = \psi b = 2\pi a$ where $2a = 0{\cdot}15$ m, opening angles $\psi = 2\pi(b = a)$, $\pi(b = 2a)$, $\pi/2(b = 4a)$, $\pi/4(b = 8a)$, $\pi/90(b = 180a)$, wall

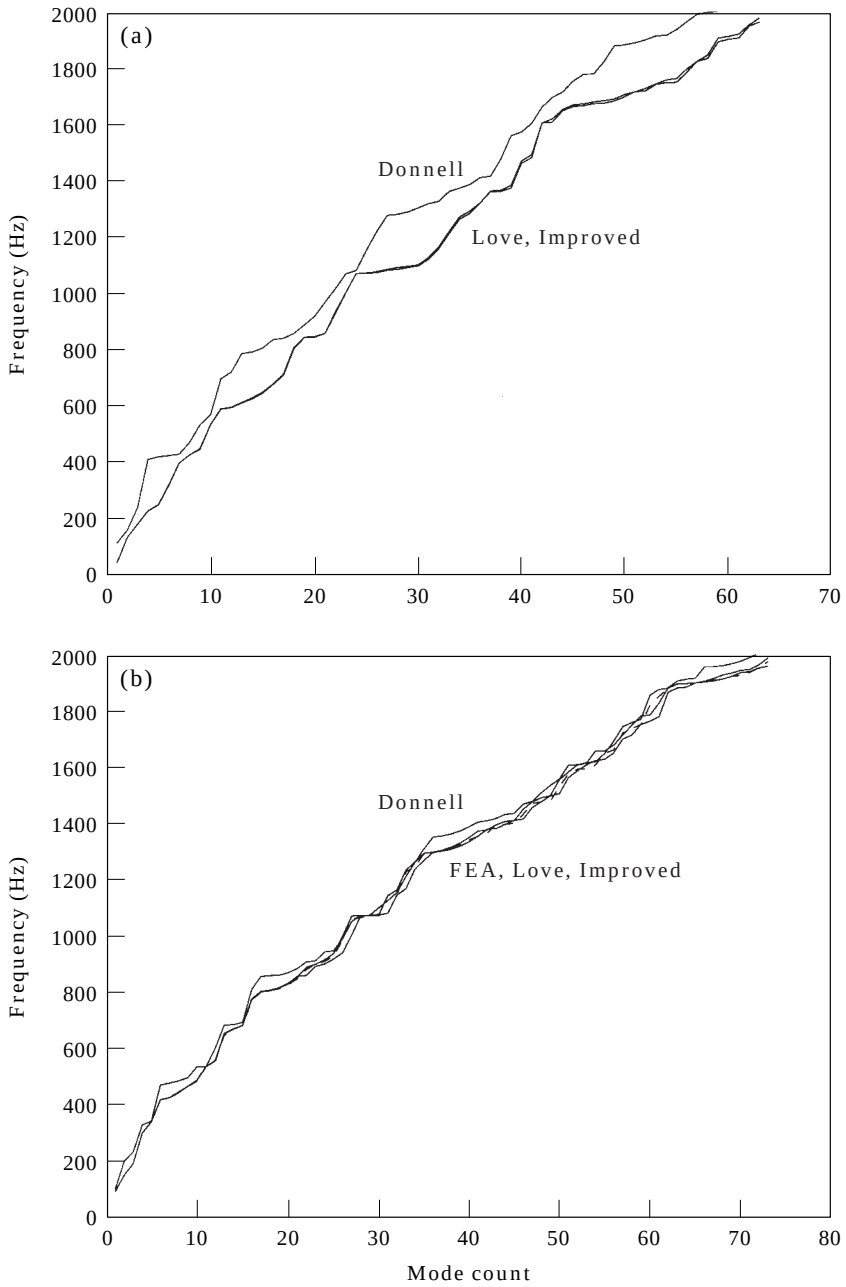

Fig. 8(a–b).

thickness $h = 0{\cdot}005$ m; and also the material properties are those of steel as for the above pipe model. These models are summarized in Table 1.

3.2. FINITE ELEMENT ANALYSIS: ELEMENT FORMULATION

For the FE analysis a parabolic quadrilateral shell element was used in both IDEAS and ABAQUS implementations. This was based on first order shell

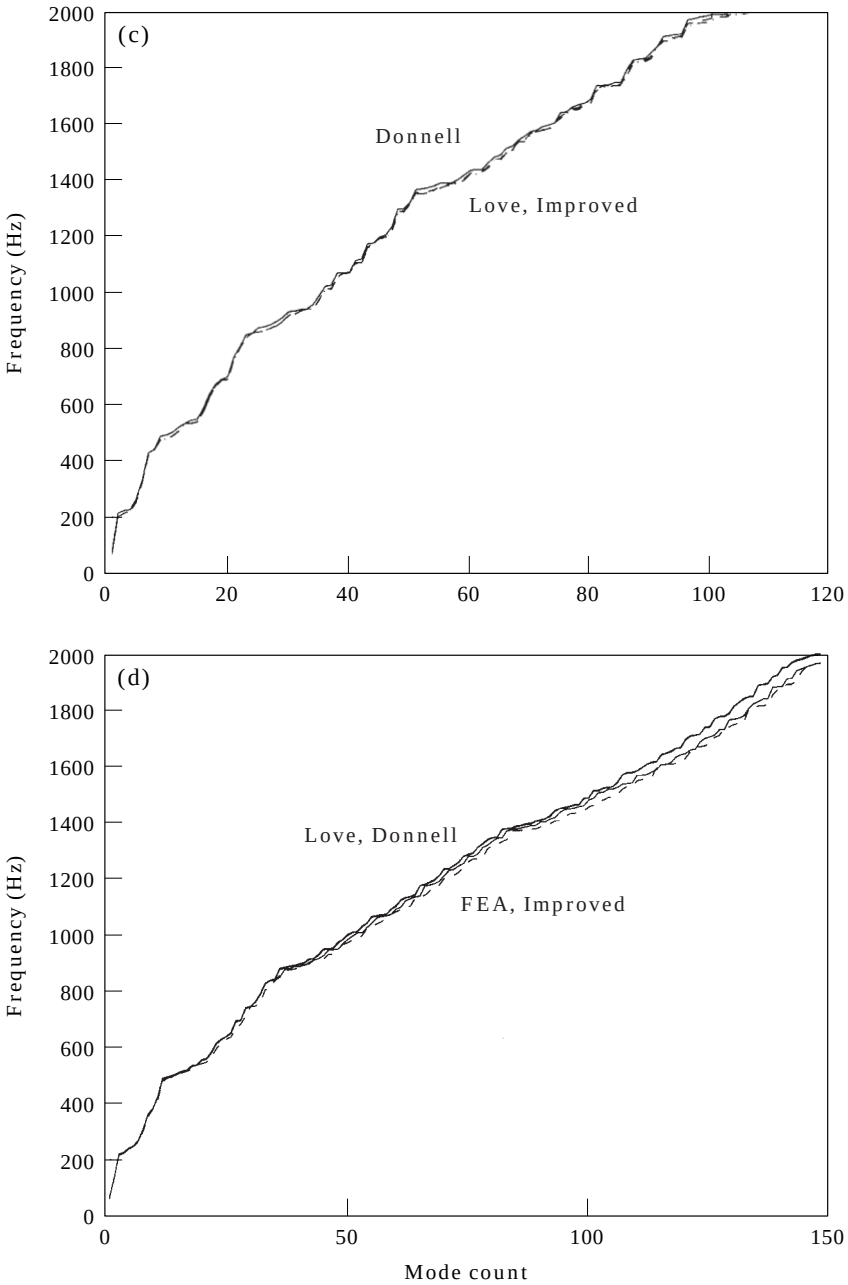

Fig. 8(c–d).

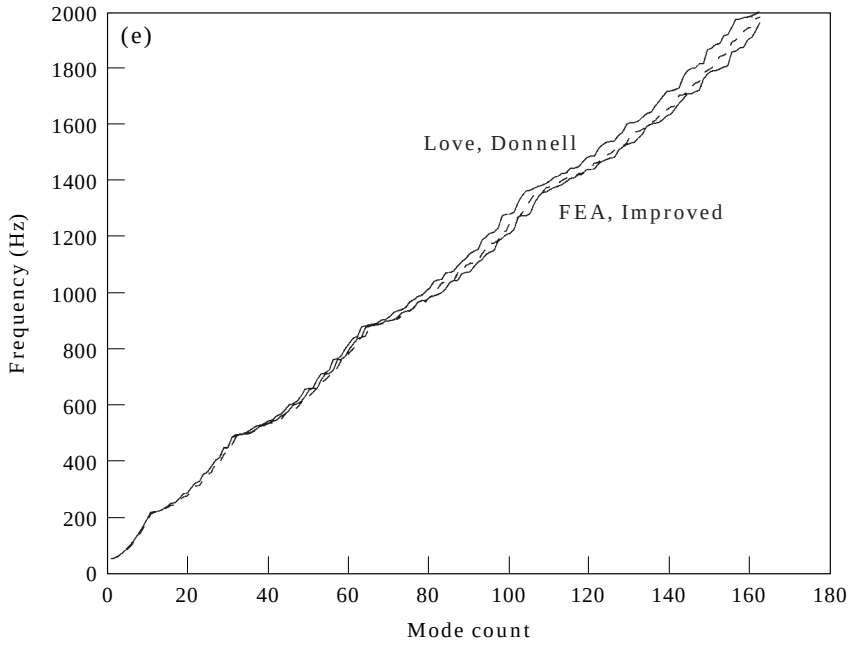

Fig. 8(e).

Figure 8. Comparison of mode count with frequency for open shells: (a) $\psi = 2\pi$; (b) $\psi = \pi$; (c) $\psi = \pi/2$; (d) $\psi = \pi/4$; (e) $\psi = \pi/90$.

equations, which include the displacements due to transverse shear strain. The formulation is a nine-node shell element as described in Huang and Hinton [14] and Hughes and Hinton [15]. A diagram of the shell element is given in Figure 3. The element has four corner nodes, four edge nodes and a central node which is internally generated and statically condensed prior to stiffness assembly. This element has five degrees of freedom at each node. When the curvature is zero the element degenerates to a plate element satisfying the Mindlin theory for plates with shear deformations.

It is worth noting that most first order shell (and plate) elements have a deficiency of membrane locking and shear locking [14], in which the transverse shear strains in the element cannot tend towards zero with decreasing thickness as they should according to thin shell theory. Hence when the shell becomes thin, thick shell elements do not necessarily converge to thin shell solutions unless specially formulated. Reduced integration is frequently employed to overcome this difficulty. In the elements used here, enhanced interpolation of the transverse shear strains is used to circumvent shear locking, and enhanced interpolation of the membrane strains is used to prevent membrane locking. Accordingly the element can be used for both moderately thick and thin shell structures. When using this element it was found that it is necessary to use the shell auto restraint facility available within IDEAS. This controls automatic restraints on the drilling degrees of freedom for shell elements whose matrix is constructed using the consistent rather than the lumped mass option. The usual implementation of shell theory in finite element codes does not produce an element stiffness term associated with the

rotational inertia about a local normal to the shell surface, the so called "drilling" degree of freedom. For doubly curved shells, a drilling freedom stiffness exists naturally due to the process of assembling contribution from adjacent elements. For cylindrical shells, however, these terms are very small.

Various techniques have been developed to deal with matrix singularity due to the lack of drilling stiffness problem [16]. Two options are available in the IDEAS

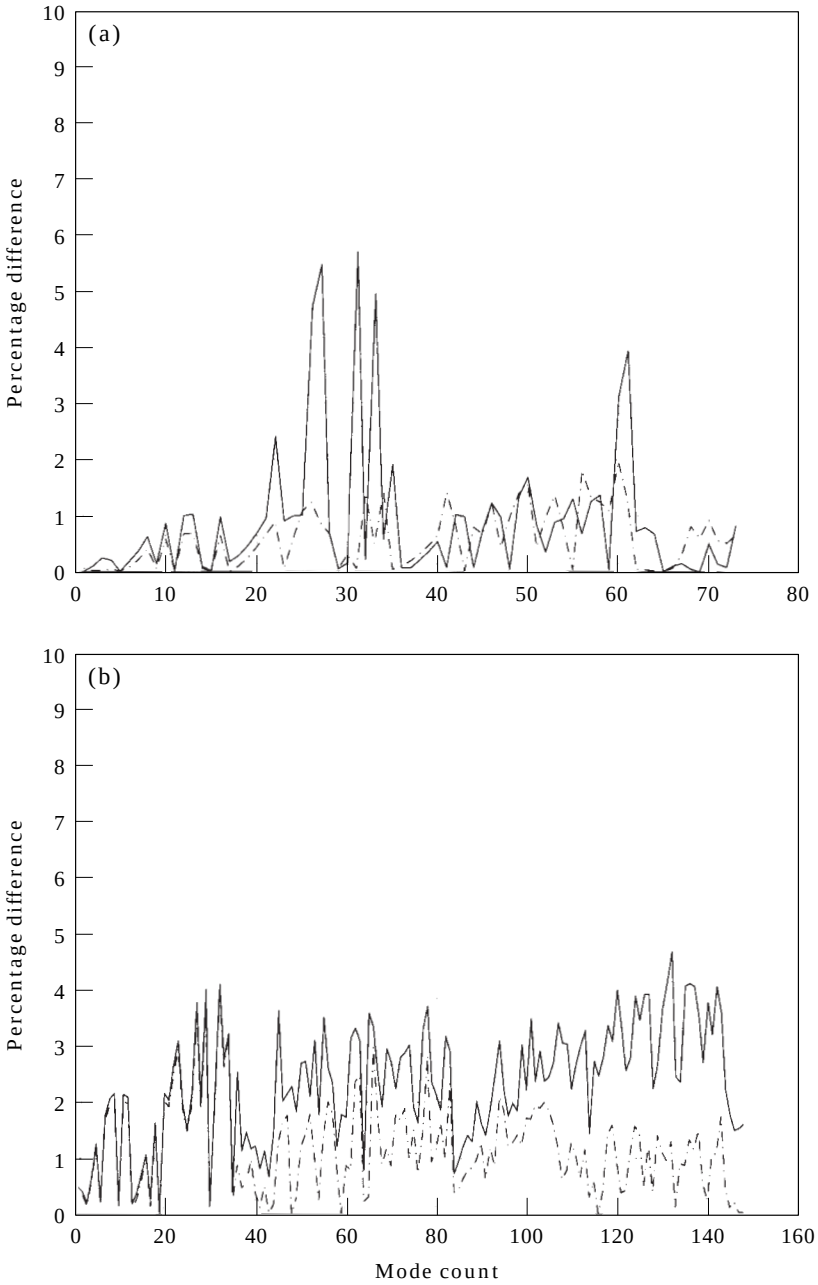

Fig. 9(a–b).

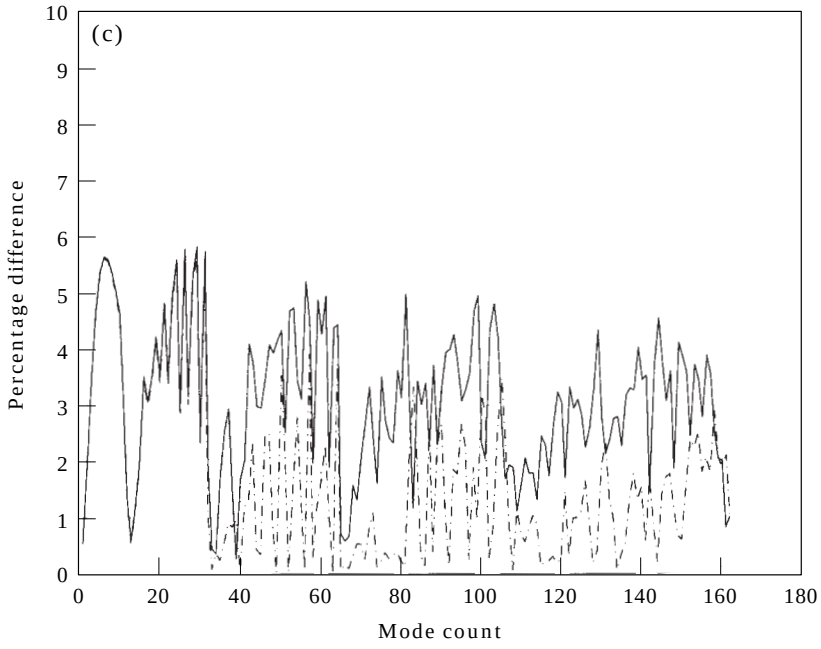

Fig. 9(c).

Figure 9. Comparison of the differences between modal frequencies of the Love —— and Improved – · – theories and FEA for open shells: (a) $\psi = \pi$; (b) $\psi = \pi/4$; (c) $\psi = \pi/90$.

software. The first option is to add a small, out-of-plane rotational stiffness to the shell element stiffness matrix using a penalty function technique, which is the default setting. The second option is to use "shell auto restraints". When "shell auto restraint" is on, the shell penalty function drilling stiffness will not be generated, but the singularity is removed by eliminating a global rotational degree of freedom, which is not in the plane of the shell. Here the cylindrical shells have curvature only in one direction, i.e., they are flat along the axial direction of the pipe and so the shell auto restraint removes singularities by eliminating redundant rotational degrees of freedom. This choice is not provided in ABAQUS, which is based on the use of lumped mass matrices.

3.3. NATURAL FREQUENCIES AND MODE SHAPES

3.3.1. *Results for the pipe models*

The natural frequencies for the axisymmetric modes ($n = 0$) and the circumferential modes $n = 1, 2, 3$, are given in Table 2 for each of the first three longitudinal modes $m = 1, 2, 3$, where these fall below a frequency of 2 kHz. No breathing modes are found below 2 kHz since the ring frequency for such a pipe occurs at 11·4 kHz. The numbers in parentheses at the top of the columns of FE results indicate the number of nodes in the models. The r indicates a consistent mass formulation with the auto restraint option switched on. The results for the ABAQUS analysis are designated (A), the others being obtained from IDEAS.

Axisymmetric modes ($n = 0$). It is immediately apparent from Table 2 that each of the theories and the FE analysis give results which agree to three significant figures for the axisymmetric modes. The best agreement is between the improved theory and the finite element model with 3148 elements, for the torsional modes given in Table 2 (as might be expected), while the longitudinal modes are best matched with FE by either Donnell's or Love's theories (which are identical in this

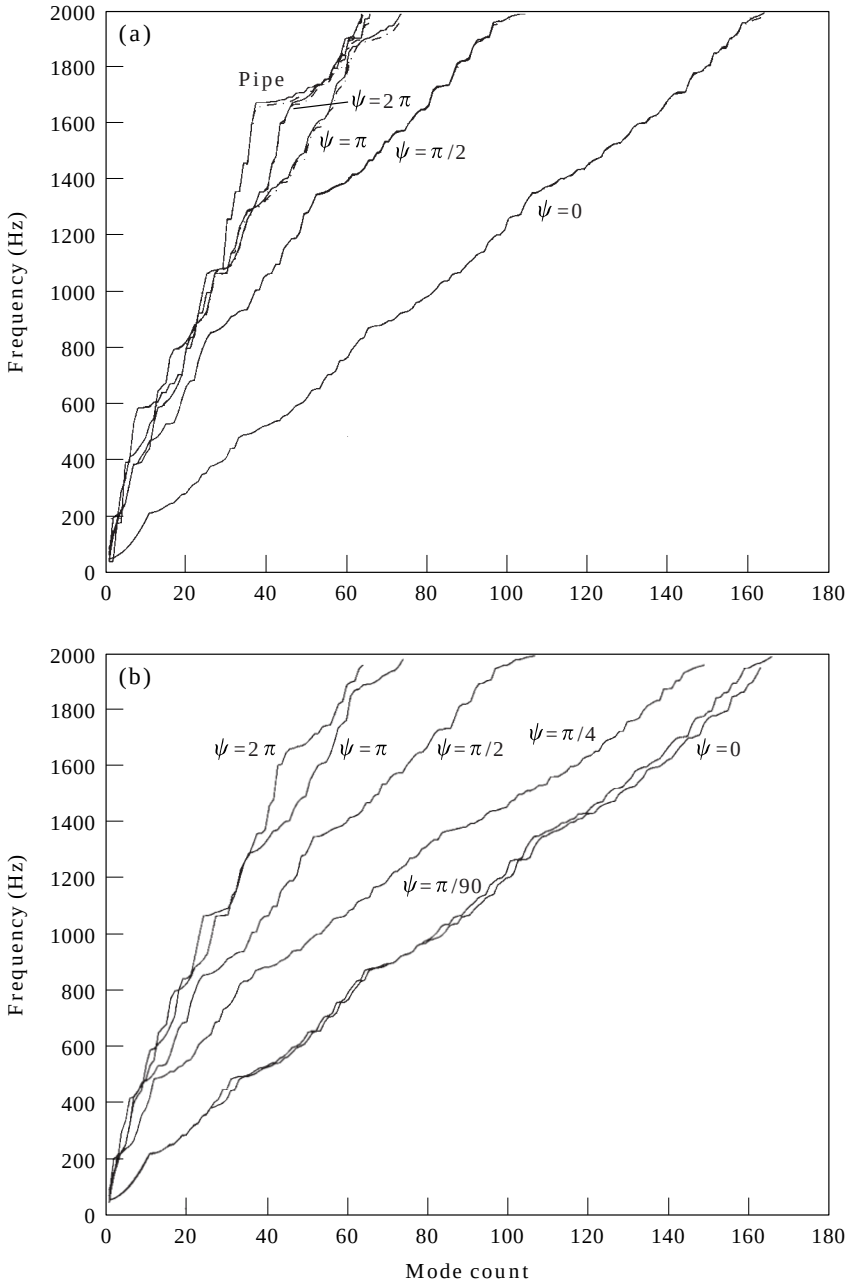

Fig. 10(a–b).

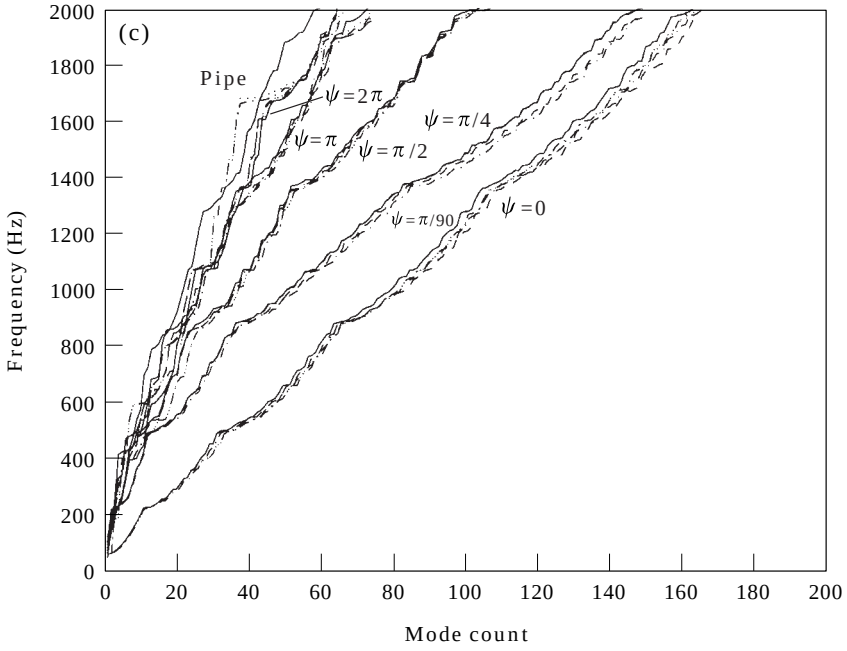

Fig. 10(c).

Figure 10. Effect of curvature on the mode count versus frequency for (a) FE models; (b) Improved theory; (c) Donnell, Love, the improved theory and FE models. (a) – · –, FEA IDEAS; ——, FEA-ABAQUS; (b) ——, Donnell; (c) - . - , Love, – – –, Improved; – · –, FEA-IDEAS; . . . . , FEA-ABAQUS.

case). The differences in all cases are however small, being at most one part in 200.

General n and m. From the table, it is seen that Donnell's theory exhibits poor agreement with either of the other two theories and the FE analysis. As pointed out by Leissa in his monograph [1], most of the extensional theories such as Donnell's are completely inadequate for low circumferential number n, e.g., $n = 1$ in the case of long shells, $L/ma \geqslant 20$. The integrands in formulating the Hamiltonian are dominated by the longitudinal bending energy [18] at low circumferential mode numbers (except when $n = 0$); this is inadequately represented by Donnell's theory due to elimination of the transverse shearing stress resultants in the equations of motion. One notes, however, that the percentage difference between Donnell's theory and the others decreases as the circumferential mode number n increases. In general the best match between the FE and the analytical theories is with the improved theory, again as expected.

It is interesting to note that the best agreement between the results from FE and the shell theories was obtained by using a lumped mass rather than a consistent mass formulation for the FE. The consistent mass matrix formulation uses the same finite element interpolation functions as is used to construct the stiffness matrix, resulting in a banded matrix whose structure is identical to that of the stiffness matrix. A lumped mass formulation leads to a diagonal mass matrix. For structural vibration problems, mass lumping softens the discretized model. This softening can sometimes improve the accuracy of the natural frequencies [19]. The

first column of FE (designated *r*) results gives the modal frequencies obtained with the consistent mass formulation and the shell auto restraint option switched on, while the second FE column gives the same analysis with a lumped mass formulation. All other features of these two models were the same. Note that using a consistent mass formulation without shell auto-restraint resulted in the occurrence of many unphysical spurious modes. This behaviour is noted in the literature accompanying the software used. As can be seen from the table, the use of the consistent mass formulation together with the shell auto-restraint on leads to slightly higher modal frequencies for general n and m, in most cases. When using the lumped mass formulation, the modal frequencies are closer to those for the improved theory, which are expected to be the most accurate. The last but one FE column shows the results for the FE model with a larger number of elements, where again the lumped mass formulation was used. The modal frequencies of the two lumped mass models are very close within this range of frequencies, giving some confidence in the results achieved. Reassuring results are also achieved by using similar models with the same number of parabolic quadrilateral shell elements implemented in ABAQUS. The corresponding frequencies are shown in the last FE(A) column. The insignificant differences in the frequencies between this and the previous sets are mainly ascribed to the different eigensolution algorithms rather than the shell models. (The last set utilizes the subspace iteration method when using the Householder and Q–R algorithm for the reduced eigenproblem executed in ABAQUS; whilst the others are obtained by the Lanczos method, when using the Rayleigh–Ritz procedure with the M-orthonormal basis of the Krylov subspace constructed from an orthogonal set of Lanczos vectors.)

Lumped mass formulations were therefore adopted for all the other FE models used here.

Figure 4 shows the total mode count with frequency for each of the theories and the FE models. The inaccuracy of the Donnell's theory for such a problem is apparent. The marked changes in the modal density, visible as gross changes in overall gradient in Figure 4, can be attributed to the threshold frequencies for the $n = 2$ and $n = 3$ circumferential modes. Figure 5 shows the difference in frequency between Love's theory, the improved theory and the FE model with the largest number of elements (3148), plotted against mode number. In general, the improved theory gives close results to the FE data.

3.3.2. *Results for the open shell models*

By holding the length of the curved side of the open shell constant and therefore the surface area constant, it is possible to investigate the effects that the radius of curvature has upon the normal mode dynamics of the structure, without the complicating effects of increasing mass. The FE models used for this study all use the parabolic shell elements described above, with meshes of 900 elements (12 by 75 elements) as for the simple pipe model. The open shells are supported such that the displacements normal to the shell plane are not allowed at the shell edges; hence the only "axisymmetric" modes which occur are the torsional modes. Figure 6 shows the deformed FE mesh ($\psi = \pi/4$) for the $m = 2$, $n = 1$ mode, to give an idea of the relative element distortion in the model with 900 elements.

Figures 7(a)–(f) show the evolution of the $n > 0$ modal frequencies as the radius of curvature of the shells change from that of a pipe to that of an almost flat plate. Figure 7(a) is for the closed pipe, shown for comparison. These results are based on the improved theory. By taking those of Figure 7(b) ($\psi = 2\pi$, but still an open shell) to be most pipe-like an those of Figure 7(f) ($\psi = \pi/90$) to be most plate-like, it is possible to examine the transition from a curved to a flat structure (see Figure 2). For a pipe at low frequencies (relative to the ring frequency), for each circumferential mode number n, the evolution of the modal frequency with increasing longitudinal mode number m (which corresponds to the number of longitudinal half waves) is such that the lines of circumferential mode numbers cross, as in Figure 7(b); while at the other extreme, i.e., for plates, they do not, as in Figure 7(f). Transitional behaviour from pipe to plate can be seen in Figures 7(d)–(e). It is interesting to note that the frequency at which this transition occurs correlates reasonably well with the "ring frequency for such a structure (which can be found in Table 1), although strictly speaking the ring frequency has no meaning in the context of an open structure when all edges are simply supported.

Figures 8(a)–(e) give the mode counts for each of the theories, for each of the open shells (where a FE analysis was performed, namely for $\psi = 2\pi$, $\psi = \pi$, $\psi = \pi/2$, etc., this is also plotted for comparison). As can be seen, as the radius of curvature of the shell increases (i.e., the curvature becomes smaller) the differences between Donnell's and Love's theory diminish, until by Figure 8(d) the differences between these theories are negligible. The reason for this is the decreasing size of the term $\varepsilon = h^2/(12b^2)$ in the governing differential equations (7) and (9). As this term becomes smaller with increasing radius of curvature, Donnell's theory tends to Love's theory. However, as can be seen from Figure 8(e), significant differences still exist between the improved theory (and FE) and Love's/Donnell's theory for an almost flat plate at large mode numbers. This must be attributed to transverse shear and rotary inertia effects.

Figure 9(a)–(c) show the percentage differences between each of the modal frequencies of Love's theory and Donnell's theory and the FE model for each of the curved shells for which the FE analysis was carried out. In each case the modal frequencies of the improved theory lie closer to the FE modal frequencies than Love's theory, as expected.

Finally, Figure 10 illustrates the evolution of the mode count versus frequency with changing curvature for the various models. The global evolution towards a flat plate with decreasing curvature can clearly be seen.

3.4. COMMENTS ON THE USE OF FE ANALYSIS

In the finite element results based on the IDEAS software, we noticed that the consistent mass plus shell auto-restraint feature slightly modified the modal frequencies, even for the lowest frequency mode. These errors were commonly of greater magnitude than the differences between the various shell theories used.

Another point concerning the accuracy of the FE results is that at high modal numbers the error in the calculation of the modal frequency is often greater than the difference between successive modes, and so the modes do not appear in their correct order. This is particularly noticeable for a structure such as a pipe, in which

modes should appear in pairs [as discussed following equation (14)] but which often appeared noticeably split by several interposing modes. In the FE analysis performed here, it was found that pairs of modes only agreed well when the residuals calculated after the eigenanalysis were less than one part in 10^5. However, as long as the detailed vibrational behaviour of the structure is not required for a large number of modes the FE analysis performs reasonably well.

The final comment relates to CPU time. The large FE model for the pipe took three and a half days of cpu time to solve on a Silicon Graphics R4400 workstation. The analytical results for the equivalent improved theory took only five minutes on the same machine.

4. CONCLUSIONS

This brief review has shown the effects of adopting different sets of assumptions on the solutions generated for pipes typical of those found in modern offshore structures. It is seen that for appropriate boundary conditions an improved theory can be set up and solved very much more rapidly than by using a finite element approach. Moreover, such methods give greater insight into the effects of parameter changes on the behaviour of pipes and, additionally, can provide higher order modes in the correct sequence and allow for degenerate groups of modes. The example studied shows the large number of elements needed in a FE model, if it is to recover accurately the higher order modes required for studying the fatigue lives of typical piping runs subjected to high frequency excitation.

REFERENCES

1. A. W. Leissa 1973 *Vibrations of Shells* NASA-SP-288. Washington, DC: U.S. Government Printing Office.
2. C. R. Calladine 1983 *Theory of Shell Structures*. Cambridge University Press.
3. A. E. H. Love 1888 *Philosophical Translation of the Royal Society of London* (*Ser. A*) 495–546. The small free vibrations and deformations of a thin elastic shell.
4. L H. Donnell 1933 *N.A.C.A. Report* No. 479. Stability of thin walled tubes under torsion.
5. W. Flügge 1962 *Stresses in Shells*. New York: Springer.
6. A. I. Lur'ye 1940 *Prikl. Mat. Mekh.* **4**(7), 7–34. The general theory of thin elastic shells (in Russian).
7. R. Byrne 1944 *University of California Publications in Mathematics*, *N.S.*, **2**, 103–152. Theory of small deformations of a thin elastic shell.
8. E. Reissner 1941 *Am. J. Math.* **63**, 177–184. A new derivation of the equations for the deformation of elastic shells.
9. P. M. Naghdi and J. G. Berry 1964 *J. Appl. Mech. ASME* **21**(2), 160–166. On the equations of motion of cylindrical shells.
10. E. B. Magrab 1979 *Vibrations of Elastic Structural Members*. Alphen aan den Rijn: Sjithoff & Noordhoff.
11. H. Krauss 1967 *Thin Elastic Shells*. New York: Wiley.
12. Š. Markuš 1988 *The Mechanics of Vibrations of Cylindrical Shells*. Amsterdam: Elsevier Science.
13. Lord Rayleigh 1945 *Theory of Sound*, vol. 1. New York: Dover.

14. H. HUANG and E. HINTON 1986 *International Journal for Numerical Methods in Engineering* **22**(1), 73–92. A new nine-node degenerated shell element with enhanced membrane and shear interpolation.
15. T. HUGHES and E. HINTON (eds.) 1986 *Finite Element Methods for Plate and Shell Structures Vol*. 1: *Element Technology*. Swansea: Pineridge Press; 46–61.
16. IDEAS Master Series 3 1996 Simulation: Finite Element Modeling/Model Solution, Structural Dynamics Research Corp.
17. ABAQUS/Standard User's Manual 1995, Hibbit, Karlsson & Sorensen, Inc.
18. G. B. WARBURTON 1964 *The Dynamic Behaviour of Structures*. Oxford: Pergamon Press.
19. R. D. COOK, D. S. MALKUS and M. E. PLESHA 1989 *Concepts and Applications of Finite Element Analysis*. New York: Wiley; 3rd edition.